Structure Evolution of Organic Compounds in Shale Plays by Spectroscopy (^{1}H & ^{13}C−NMR, XPS, and FTIR) Analysis

Hyeonseok Lee[2], Nuri Oncel[3], Alexandera Kukay[3], Bo Liu[1], Rajender S. Varma[4], Mohammadreza Shokouhimehr[1,5*], Mehdi Ostadhassan[1*]

[1]Key Laboratory of Continental Shale Hydrocarbon Accumulation and Efficient Development, Northeast Petroleum University, Daqing 163318, China

[2]Department of Petroleum Engineering, University of North Dakota, Grand Forks, ND 58202, United States

[3]Department of Physics & Astrophysics, University of North Dakota, Grand Forks, ND, United States

[4]Regional Centre of Advanced Technologies and Materials, Faculty of Science, Palacky University in Olomouc, Šlechtitelů 27, 783 71, Olomouc, Czech Republic

[5]Department of Materials Science and Engineering, Research Institute of Advanced Materials, Seoul National University, Seoul, 08826, Republic of Korea

*Corresponding authors' e-mail addresses:
mehdi.ostadhassan@nepu.edu.cn, mrsh2@snu.ac.kr,

Abstract

Amorphous organic matter in geomaterials also known as kerogen undergoes significant alteration in chemical structure during thermal maturation which is characterized using a combination of solid−state ^{1}H & ^{13}C−NMR, X−ray photoelectron spectroscopy (XPS), and Fourier transform infrared (FTIR) techniques. For this study, four kerogen samples (type−II) from the Bakken Formation were selected based on the differences in their thermal maturity, as well as representing the pre−oil and oil window stages as measured through organic petrology and bulk geochemical screening of the samples using programmed pyrolysis. Later, organic matter was extracted from selected aliquots for chemical spectroscopy. Results documented a systematic structural change in these four samples where the ratio of CH_3/CH_2 increased when the maturity increases, along with the presence of shorter aliphatic chain length. Furthermore, the aromatic carbon structure becomes more abundant in higher maturities and oil window stages quantified by ^{13}C−NMR, XPS, and FTIR. Also, the rate of increase in aromaticity demonstrates a considerable rift between pre−oil window and oil window stages, as verified through bulk geochemical screening of the samples with Rock-Eval 6 pyrolysis HI index. Notably, it's found that kerogen maturation causes the relatively bulky oxygen−related carbon compounds to reduce at the early stages of maturation (pre−oil window) followed by concentration of such compounds at higher maturity stages. Next, the ratio of carbonyl/carboxyl functional groups to aromatic carbon shows an increase in oil window stage while reduction of sulfur in higher maturities was detected mainly in the SO_x forms. Finally, nitrogen content of the samples is reported in a variety of forms which varied regardless of the thermal maturation. Its concluded that, the structural and chemical changes that occurs in the organic matter involves defunctionalization of heteroatom functional groups, coupled with an increase in cross−linked carbon in the residual remaining kerogen.

Keyword: Shale; Organic Compounds; Spectroscopy analysis;

1. Introduction

The abundance of organic carbon and heteroatoms in shale layers, which are deposited in source rocks in the form of organic matter, leads to the generation of hydrocarbon through thermal maturation. The solid−state organic compound (known as kerogen) of these atoms breaks down and undergoes a significant structural and compositional transformation during thermal maturation [1,2]. In this regard, the study pertaining to these changes in kerogen structure has potential to better characterize CO_2 sequestration and the enhanced oil recovery (EOR) methods [3]. However, there is a significant difficulty in understanding the mechanism of kerogen cracking coupled to hydrocarbon generation due to chemical heterogeneity and complexity of the kerogen molecular structure. Moreover, the limitation of analytical methods could not thoroughly provide quantitative molecular information of kerogen structure [4].

Kerogen characterization methods such as visual kerogen analysis (VKA) and pyrolysis (bulk geochemical techniques), are limited to the determination of the type of kerogen, maturity level, and hydrocarbon generating potential. Hence, in order to obtain the detailed structural information of kerogen, a number of spectroscopic techniques have been deployed [5−7]. The methods mentioned are destructive in addition to the limited information they can provide, thus other non−destructive methods such as Fourier transform infrared (FTIR) spectroscopy, Raman spectroscopy, X−ray photoelectron spectroscopy (XPS), X−ray diffraction (XRD), and ^{1}H & ^{13}C solid−state nuclear magnetic resonance (^{13}C−NMR) have been utilized to obtain quantitative structural information from the kerogen [5,8−10]. These direct methods can examine the solid kerogen sample without imposing any alterations so that the results would enable studying the structure and assist in building macromolecular models of kerogen though computational technique at the same time [11,12].

Organic carbon in source rocks has been investigated by the solid−state ^{13}C−NMR technique coupled with FTIR [13,14]. These spectroscopic tools can provide the qualitative and quantitative information related to both the structural assignment of carbon and the distribution of aromatic/aliphatic carbons in organic compounds in the last decade [15−17]. For studying the organic heteroatoms (oxygen, nitrogen, sulfur), FTIR and Raman are common methods employed for the analysis of functional groups in complex organic solids. However, due to the limitations of the functional groups acquired from these techniques, quantitative analysis are not adequate to

fully provide detailed structural information. In order to complement missing data, XPS has been utilized for evaluating the organic compounds by overcoming this inherent deficiency to quantify organic heteroatoms with acceptable results [18,19].

In this study, four isolated (extracted) kerogens from the mineral matrix at four different stages of natural thermal maturity from the Bakken Shale formation, from pre−oil to oil window stages, were examined by a combination of non−destructive analytical methods (^{1}H & ^{13}C−NMR, XPS, and FTIR) for chemical and structural analysis. The aim of this study was to identify structural characteristics and evolution of solid−state organic compound as it undergoes thermal maturity in nature and to discover these changes in terms of quantitative and qualitative information from chemical structures point of view. Additionally, we investigated other aspects of thermal maturation that can help us explain processes that would generate hydrocarbons from the organic compounds in the source rock.

2. Materials and Methods

2.1. Samples

Solid−state organic compound, type II kerogen samples were extracted from four different wells in the Bakken formation which is one of the largest unconventional shale oil plays in North America and is currently being studied for unconventional CO_2 EOR and sequestration [20−22]. Initially, the degree of maturity four Bakken kerogen samples (sample A−D) were examined by bitumen reflectance (%SBR_o) of the samples were examined along with bulk geochemical properties using Rock−Eval 6 pyrolysis that is summarize in Table 1. In Figure 1 and Table 1, samples A−B are at the thermally immature (pre−oil window) stage, while, samples C−D are at the peak mature (oil window) stage. It's important to note that selected kerogen samples were isolated using HCl and HF, and details of sample preparation and organic matter extraction procedure can be found in Abarghani et al. [23], and Khatibi et al. [24].

Table 1. Properties of four solid−state organic compound (kerogen) samples (type II)[a].

Sample No.	T_{max} (°C)	TOC (wt %)	HI (mg/g C)	SBRo (%)
A	428	14.56	569	0.33

B	432	15.76	531	0.49
C	449	12.69	260	0.72
D	452	16.36	171	0.94

[a]*The values were examined by the UV reflectance (%SBR$_o$) and Rock−Eval 6 with parameters: Tmax, TOC (Total organic carbon), HI (hydrogen index).*

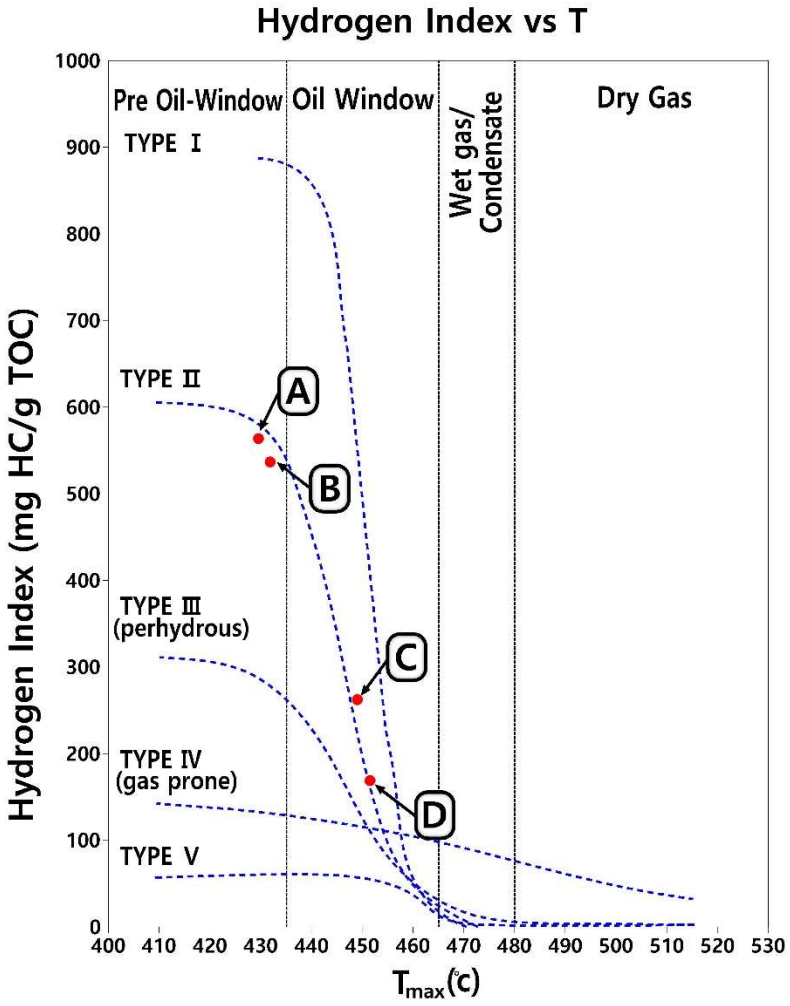

Figure 1. Selected samples A−D are following kerogen type II thermal maturity trend where Samples A−B are at the thermally immature (pre−oil window) stage, and samples C−D are at the peak mature (oil window) stage.

2.2. Solid−state ^{1}H & ^{13}C−NMR (Nuclear Magnetic Resonance)

Solid−state ^{1}H & ^{1}3C−NMR analysis was carried out using a Bruker Avance III HD spectrometer with cross polarization−magic angle spinning (CP/MAS). The kerogen sample (100−150 mg) was packed and spun at 5 kHz. A contact time of 1.5 ms and recycle delay time of 5 s were used in the cross−polarization (CP). Resonance frequencies of ^{1}H−NMR and ^{13}C−NMR were 500 MHz and

125 MHz, respectively with the spectral widths of 10 kHz and 25 kHz for ^{1}H−NMR and ^{13}C−NMR. The relative proportion of different carbon types in the samples was quantified through curve fitting of the ^{13}C−NMR spectrum, which was conducted with the ratios of Gaussian to Lorentzian distribution; the full width at half−maximum (fwhm). The details of structural parameters and assignments of chemical data shifts are presented in Table 2 [25,26].

2.3. XPS (X−ray Photoelectron Spectroscopy)

Freshly−powdered samples were pressed on indium foils and analyzed by a Al Kα (1486.6 eV) X−ray source with a pass energy of 89.5 eV and 44.75 eV for the survey and higher−resolution scans, respectively. During the XPS measurements, the pressure was kept at or below 1×10^{-9} mbar. The angle between the X−ray source, which is aligned along the surface normal, and the spectrometer is 54.7. All the XPS core−level spectra were analyzed using Augerscan and Origin software's. The core−level peaks are fitted using a Gaussian−Lorentzian (GL) function to include the instrumental response function along with the core−level line shape. The secondary electron background was subtracted using a Shirley function. We compensated charging of the sample by irradiating the sample with an electron−flood gun (5 eV) [27].

2.4. FTIR (Fourier transform infrared spectroscopy)

The infrared spectra of kerogen samples were recorded in adsorption range between 450 and 4000 cm^{-1} using a Thermo Fisher Scientific, Nicolet iS50 FTIR Spectrometer. Four kerogen samples were pulverized using a ball mill prior to characterizations. Fourier transform infrared (FTIR) spectroscopy using attenuated total reflectance (ATR) was employed to analyze kerogen extracts. Unlike transmittance FTIR, ATR does not require that kerogen samples be mixed with potassium bromide and formed into pellets under high pressure, thus reducing the time needed for the sample preparation. Kerogen samples were placed in contact with an internal reflection compound and IR spectra were obtained based on the excitation of the molecular vibrations of chemical bonds by the absorption of the light. The stretching absorptions of a vibrating chemical bond are observed at higher frequencies (wavenumbers) than the corresponding bending or bond deformation vibrations [28]. Because kerogen is rather a complex entity which limits the analysis of integrated bands in the bending vibration area, we decided to look at the C−H set of stretch vibrations

observed in kerogen samples, as proposed in previous studies [28,29]; bands of the absorption were identifying by comparison with published spectra.

3. Results and Discussions

3.1. Solid−State ^{1}H & ^{13}C−NMR

Aromatic and aliphatic proton regions of ^{1}H–NMR spectrum provide relatively qualitative information of hydrogen at different maturity levels [26]. From the acquired spectra in Figure 2 (left), aromatic and aliphatic protons exist in the 6.4–8.3 ppm range and 0.5–4.3 ppm range, respectively. The ^{1}H−NMR spectra of sample A–D in Figure 2 (left) show a broad asymmetric line centered around 0–1 ppm (centered at 0.64, 0.24, 0.54, and 0.91 ppm respectively). Sample A (immature) has strong intensity in the range of the aliphatic protons between 0.5 to 4.3 ppm; the peak at 4.15 ppm indicates that the ratio of aliphatic protons to the aromatic ring is higher than the rest of the samples. In this regard, the results reveal that the shape of ^{1}H−NMR spectrum becomes sharp as the degree of maturity increases, which manifests the number of protons attached to aliphatic carbon reduces. However, the ^{1}H−NMR spectra output as a result of highly overlapping peaks were difficult to distinguish and quantify structural formation of hydrogen which has been a problem in the past [30,31]. Therefore, we decided to rely solely on the result of ^{13}C−NMR to extract quantitative information of carbon related structures.

The ^{13}C−NMR spectra of kerogen samples mainly reveal three regions: the aliphatic region at 0–90 ppm, the aromatic region at 100–165 ppm, and carbonyl/carboxyl carbon region at 165–220 ppm. Figure 2 (right) illustrates that the ^{13}C−NMR spectrum of immature kerogen is distinct from the mature one in the range of the aromatic carbons between 90 to 220 ppm. Highly matured kerogen has stronger intensity in ^{13}C–NMR spectrum related to aromatic structure. To acquire the details of carbon structural information, overlapping peak resolving of the ^{13}C–NMR spectra is deconvoluted by the fitting procedure. The relative areas calculated by the peak fitting, which represent the relative amount of the carbon−containing functional groups, are listed in Table 2.

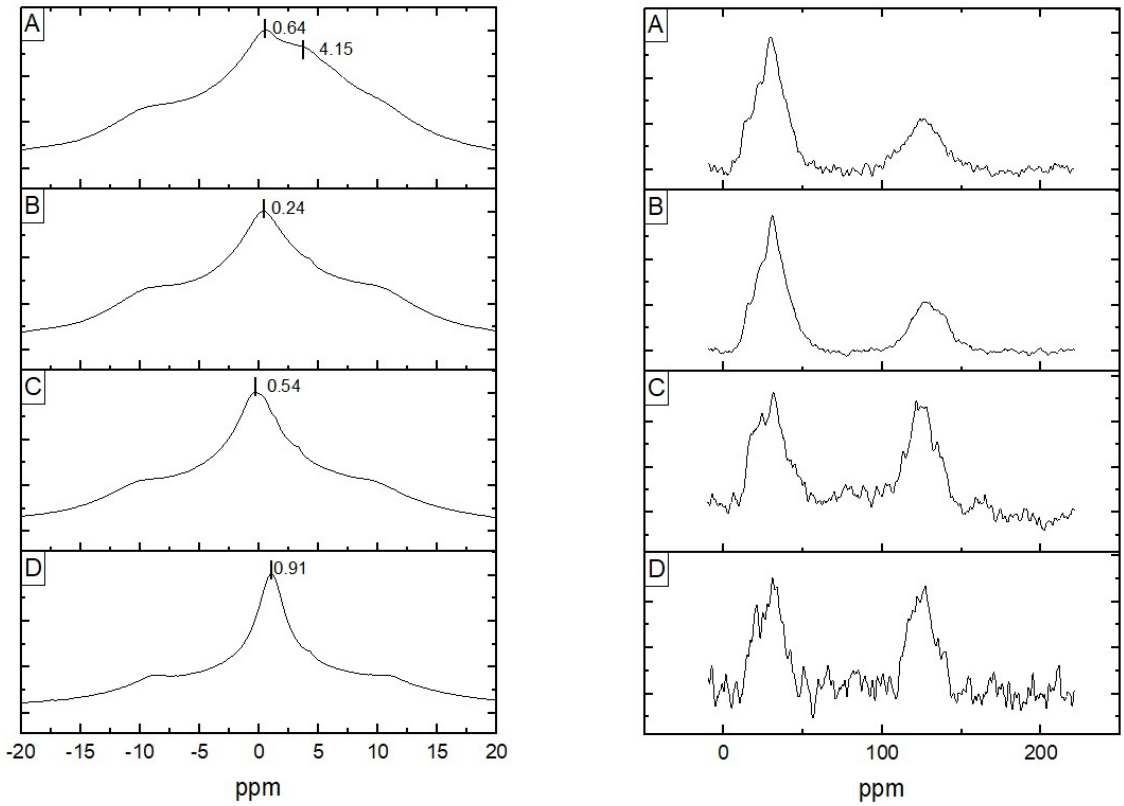

Figure 2. ^{1}H−NMR (left) and ^{13}C−NMR (right) spectra of kerogen samples of samples from A-D.

Table 2. Structural parameters and assignments from ^{13}C−NMR spectra of the samples[a].

	f_{al}^{1} (0−16)	f_{al}^{2} (16−25)	f_{al}^{H1} (25−36)	f_{al}^{H2} (36−51)	f_{al}^{O1} (51−75)	f_{a}^{O2} (75−90)	f_{ar}^{H} (90−129)	f_{ar}^{B} (129−137)	f_{ar}^{S} (137−150)	f_{ar}^{P} (150−165)	f_{a}^{C} (165−220)
A	0.080	0.050	0.240	0.20	0.056	0.02	0.23	0.032	0.047	0.015	0.030
B	0.075	0.064	0.196	0.19	0.057	0.03	0.25	0.035	0.052	0.024	0.027
C	0.070	0.067	0.165	0.10	0.049	0.05	0.34	0.037	0.061	0.029	0.032
D	0.056	0.066	0.120	0.10	0.051	0.04	0.37	0.045	0.084	0.030	0.038

[a]All ^{13}C chemical shift (ppm) were measured and assigned in carbon structural functionalities (f_{al}^{1}: aliphatic methyl, f_{al}^{2}: aromatic methyl, f_{al}^{H1}: methylene, f_{al}^{H2}: quaternary carbon, f_{al}^{O1}: methoxyl/aromatic methoxyl, f_{al}^{O2}: aliphatic carbon bonded to oxygen in cyclic hydrocarbon, f_{ar}^{H}: protonated aromatic carbon, f_{ar}^{B}: bridgehead aromatic carbon, f_{ar}^{S}: branched aromatic carbon, f_{ar}^{P}: oxy−aromatic carbon, and f_{a}^{C}: carbonyl/carboxyl carbon) [25,26].

As shown in the $^{13}C-NMR$ analysis (Table 2), with increasing thermal maturity, the aliphatic functional groups (0–90 ppm) exhibit a reduction trend in the relative amount of carbon, whereas the aromatic carbon groups (90–165 ppm) increase. This behavior is in a agreement with $^{1}H-NMR$ spectra in Figure 2 (left). The nonpolar alkyl carbons (0–51 ppm) generally diminish with the degree of maturity, except the aromatic methyl (f_{al}^{2}) group which could be reflected by the increase of aromatic carbon. In addition, we infer that loss of oxygen at the early stages of maturation is due to a comparatively weak bond between oxygen–related carbon and kerogen backbone [19]. However, the results revealed that there isn't any meaningful relationship between oxygen–related carbons (f_{al}^{O1}, f_{al}^{O2}, f_{a}^{C}) and thermal maturity. We understand that, because the stoichiometry of oxygen–related signal is uncertain [29], it is difficult to estimate the accurate values concerning oxygen–related carbon. However, this study additionally investigated the changes of oxygen–related carbon with XPS and FTIR during the maturation, and based on the results given in Table 2, the evaluations of the carbon skeletal structure were correlated to the maturity levels of kerogen that is later discussed.

3.2. XPS

Different types of organic carbon and oxygen forms were determined by analyzing the carbon (1s) peak. In each sample, we determined four peaks located approximately at 285 eV, 286 eV, 287.5 eV, and 289 eV after fitting the XPS carbon (1s) signal. The peak at 285 was attributed to both aromatic and aliphatic carbon. The amount of aromatic carbon was estimated using the XPS technique for $\prod$ to $\prod^{*}$ signal intensity as has been used previously [32]. This confirms that the highly mature kerogen has an abundance of aromatic carbon structure as revealed in the solid−state ^{1}H & $^{13}C-NMR$ results. The peaks at 286 eV, 287.5 eV, and 289 eV originate from carbon atoms bound to one oxygen atom by a single bond (C−O), carbon atoms bound to two oxygen atoms (O=C−O), and carbon atoms bound to one oxygen atom by two bonds (C=O), respectively. In the most mature stage (sample D), the results show a relatively large amount of enrichment for oxygen−related carbon, whereas the rest of the samples (A−C) exhibit comparatively similar amount of oxygen−related carbons in kerogen structure (Table 3).

Organic nitrogen and sulfur information in kerogen structure was also obtained using XPS curve fitting methods, which at different energy positions are used to fit with the XPS N 1s and S 2p spectra, respectively. Nitrogen (1s) kerogen spectra were curve−resolved using four peaks at fixed

energy positions of 397, 398.6, 399.4, 400.2, and 401.4 eV. Considering the organic sulfur (2p), the binding energy between 162−165.7 eV is assigned to pyrite, aliphatic and aromatic sulfur, and sulfoxide in XPS S 2p spectrum having $2p_{3/4}$ and S $2p_{1/2}$. The peaks at 168.0 (± 0.5) to 170.5 (± 0.5) eV can be indexed to S $2p_{3/4}$ and S $2p_{1/2}$ of SO_x (sulfate/sulfite/sulfone). The peak locations, which are a little higher than the expectation, could be affected by the poor electrical contact in surface oxidation; the accumulation of positive charge shifts peaks toward higher binding energy. Because the peaks at 168.0 and 160.5 eV are overlapped and have also been observed in previous literature, we consider that the summation of this region presents the SO_x assignment of sulfate, sulfite, and sulfoxide [5,29]. Table 3 exhibits the details of quantitative structural parameters based on the curve fitting into different components of the selected kerogen samples (A−D).

Table 3. Structural parameters and assignment for the XPS spectra of the kerogen samples.

Elemental	**Functionality**	**Binding energy (eV)**	**Mole percent**			
			A	**B**	**C**	**D**
C1 1s	Aliphatic	248.8	49	58	40	16.4
	Aromatic[a]		39	34	50	55
	C−O	286	1.2	0.6	1.4	23.1
	C=O	289	7.3	4.6	2.8	2.3
	O−C=O	287.5	3.5	6.2	11	6.2
N 1s	Nitride	397	−	19.8	24.8	12.5
	Pyridinic	398.6	−	16.4	15.7	22.2
	Quaternary	401.4	−	23.6	10.6	31.3
	Amino	399.4	−	20.6	42	9.8
	Pyrrolic	400.2	−	19.6	6.8	24.2
S 2p	Pyrite (FeS_2)	162	13.5	16.4	6.2	0.5
	Aliphatic	163	10.1	1.7	1.5	11.9
	Aromatic	164	20.1	1.3	3	14.9
	Sulfoxide	165.7	0.3	0	0	5.3
	SO_x[b]	168−170.5	58.0	80.6	89.4	67.4

[a]*The amount of aromatic carbon was estimated by the technique of XPS* $\prod$ *to* $\prod^*$ *signal intensity in previous literature [34].*

[b]*The summation of the region presents the* SO_x *assignment of sulfate, sulfite, and sulfoxide.*

3.3. FTIR

The intensities, depicted in Figure 3, correspond to the asymmetric and symmetric stretching and bending of the C−H/C=O/C=C−C bonds about the central carbon atom on a relative basis in the spectra of kerogen samples. The reason for the overlapped original spectra is due to the same amount of energy, which is required for several vibrations. Therefore, IR structural evaluations have been established from acquired spectra documented in earlier studies [2,26]. To find the intensities at desired frequencies, the FTIR spectrum area 1800−1500 cm^{-1} and 3200−2700 cm^{-1} was fitted by the Fourier self−deconvolution [33]; the coefficients of determination (R^2) of the peak fitting for the region in all spectra were found between 0.994−0.996.

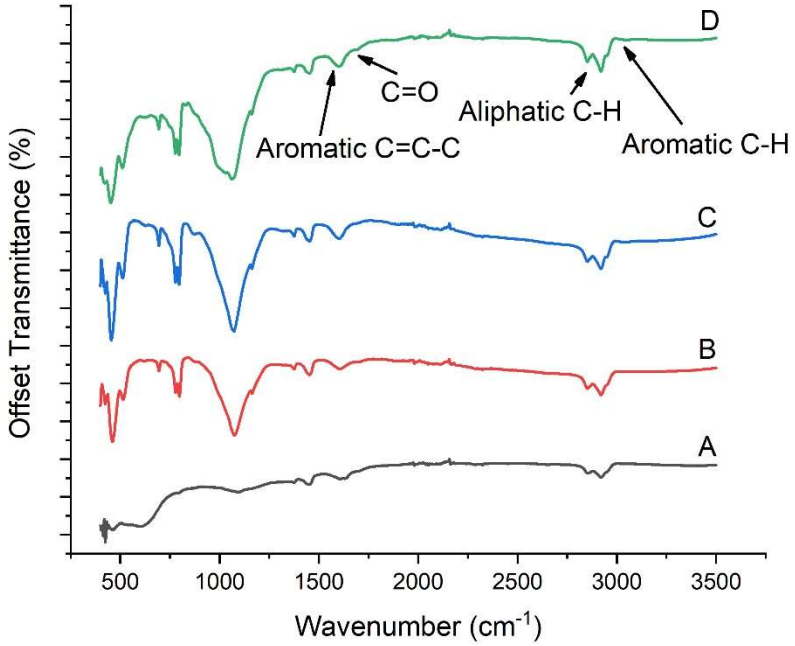

Figure 3. FTIR spectra of kerogens with increasing maturity exhibits the changes in the C−H stretch vibration area (2800−3200 cm^{-1}), aromatic C=C−C ring stretch vibration area (1615−1580 cm^{-1}), and Carbonyl/Carboxyl group vibration area (1650−1750 cm^{-1}).

Here, we examined the C−H stretching band intensities for CH_3, CH_2, aromatic ring CH, aromatic ring C=C−C, and C=O based on the deconvolution results. Four indices (CH_3/CH_2 ratio, aromaticity, A−factor, and C−factor) were used to evaluate the structural characteristic of each different kerogen. The CH_3/CH_2 ratio [$I_{(2970–2950)}/I_{(2935–2915)}$] indicates the average chain length of aliphatic and the degree of chain branching. Aromaticity [$I_{(3130–3070)}/(I_{(2970–2950)}+I_{(2935–2915)})$]

represents the degree of aromatic structure versus aliphatic chain structure. The A−factor [$I_{(2935-2915)}/(I_{(2935-2915)}+I_{(1615-1580)})$] and C−factor [$I_{(1750-1650)}/(I_{(1750-1650)}+I_{(1615-1580)})$] describe the relative amount of aliphatic carbon and oxygenated carbon to aromatic carbon, respectively [26] and all indices are calculated through integrating the area under the curves. When the maturity increases, the CH_3/CH_2 ratio acquired demonstrates that the aliphatic chain length is comparatively shorter, and the branching is developed. Restated, highly mature kerogen has more aromatic ring contribution and less methyl/methylene involvement with the expected increase in aromatic structure (aromaticity index). The observed trends corroborate findings from previous studies where, during the maturation, chemical structure changes have been drawn into shorten aliphatic chain length and expanding aromaticity [26]. The result of A−factor, regarding the relative amount of aliphatic to aromatic carbon, indicates that there is generally a decreasing trend over the degree of maturation. Oxygen−related information (C−factor) reveals that the ratio of oxygen−related carbon to aromatic carbon initially decreases (immature stage), then rises at the mature stage advances; the comparative details of the indices are discussed in more details in the discussion section.

3.4. Carbon Structural Changes

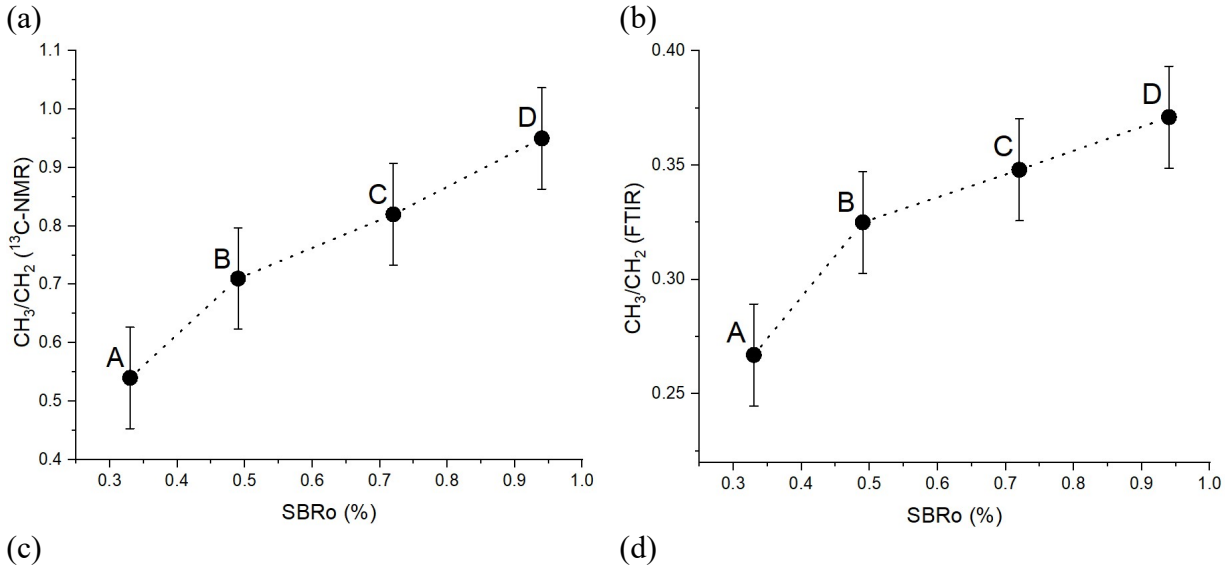

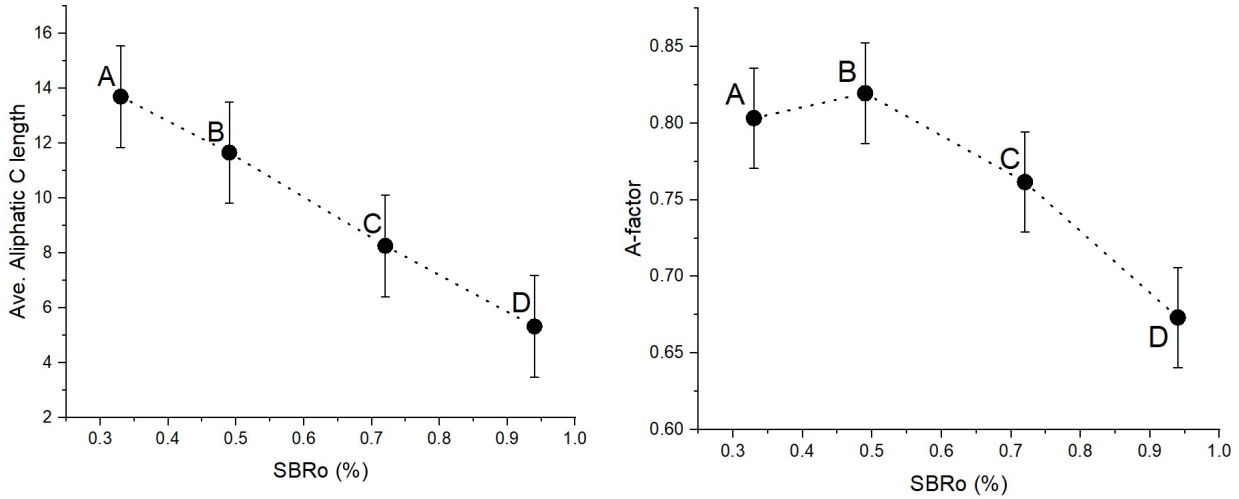

Figure 4. The aliphatic carbon structure changes by thermal maturity. The ratio of methyl/methylene is estimated from (a) ^{13}C−NMR [($f_{al}^{1} + f_{al}^{2}$)/ f_{al}^{H1}] and (b) FTIR [$I_{(2970-2950)}/I_{(2935-2915)}$] results. (c) Average aliphatic carbon chain length by ^{13}C−NMR [($f_{al}^{1} + f_{al}^{2} + f_{al}^{H1} + f_{al}^{H2} + f_{al}^{O1} + f_{al}^{O2}$) / f_{ar}^{S}]. (d) A−factor by FTIR [$I_{(2935-2915)}/(I_{(2935-2915)}+I_{(1615-1580)})$]. Error bars represent standard errors.

The ratio of CH_3/CH_2 from ^{13}C−NMR have a similar order of increase to those obtained from the FTIR analysis when the maturity increases (Figures 4a−b), which is consistent with the previously described data from type II kerogen structure [34]. This growth of CH_3/CH_2 ratio could be the evidence of chain cleavage coupled with hydrocarbon generation. While kerogen maturation occurs naturally, the molecular structure of this macromolecule evolves through bond−breaking and bond−forming, under changing physical conditions (temperature, pressure, and time) of the subsurface [1,35]. In terms of carbon to carbon (C−C) bond in the kerogen structure, bond−dissociation energy (BDE) between α and β carbon is weaker than one between α and aromatic carbon [33,36]. Also, short branching carbon (such as methyl) to carbon in the backbone structure has less BDE than longer chain carbon [20,34]. It appears that kerogen samples of the Bakken shale play also follow this mechanism which indicates higher ratio of CH_3/CH_2 during thermal maturation as shown in Figures 4a−b. In addition to the ratio of CH_3/CH_2, the average aliphatic carbon length and the amount of aromatic carbon follows this trend too. Figure 4c explains that the average length of aliphatic carbon reduces as the maturity increases meaning thereby that thermal maturation accompanies the structural changes in kerogen with both shorter aliphatic chain and higher ratio of CH_3/CH_2, as delineated by FTIR and ^{13}C−NMR.

Also, the A−factor calculated through FTIR data (Figure 4d) shows that relative ratio of aliphatic to aromatic carbon generally decreases in accordance with the shape of the ^{1}H−NMR spectrum apart from sample B that has the highest overall value. The lower A−factor value of sample A than sample B was expected because the ratio of CH_3/CH_2 increases and aliphatic chain length becomes shorter. This could be explained by the fact that the amount of aromatic carbon in sample B is relatively lower than was expected which is supported by the analysis of aromatic carbon presented in Figure 5.

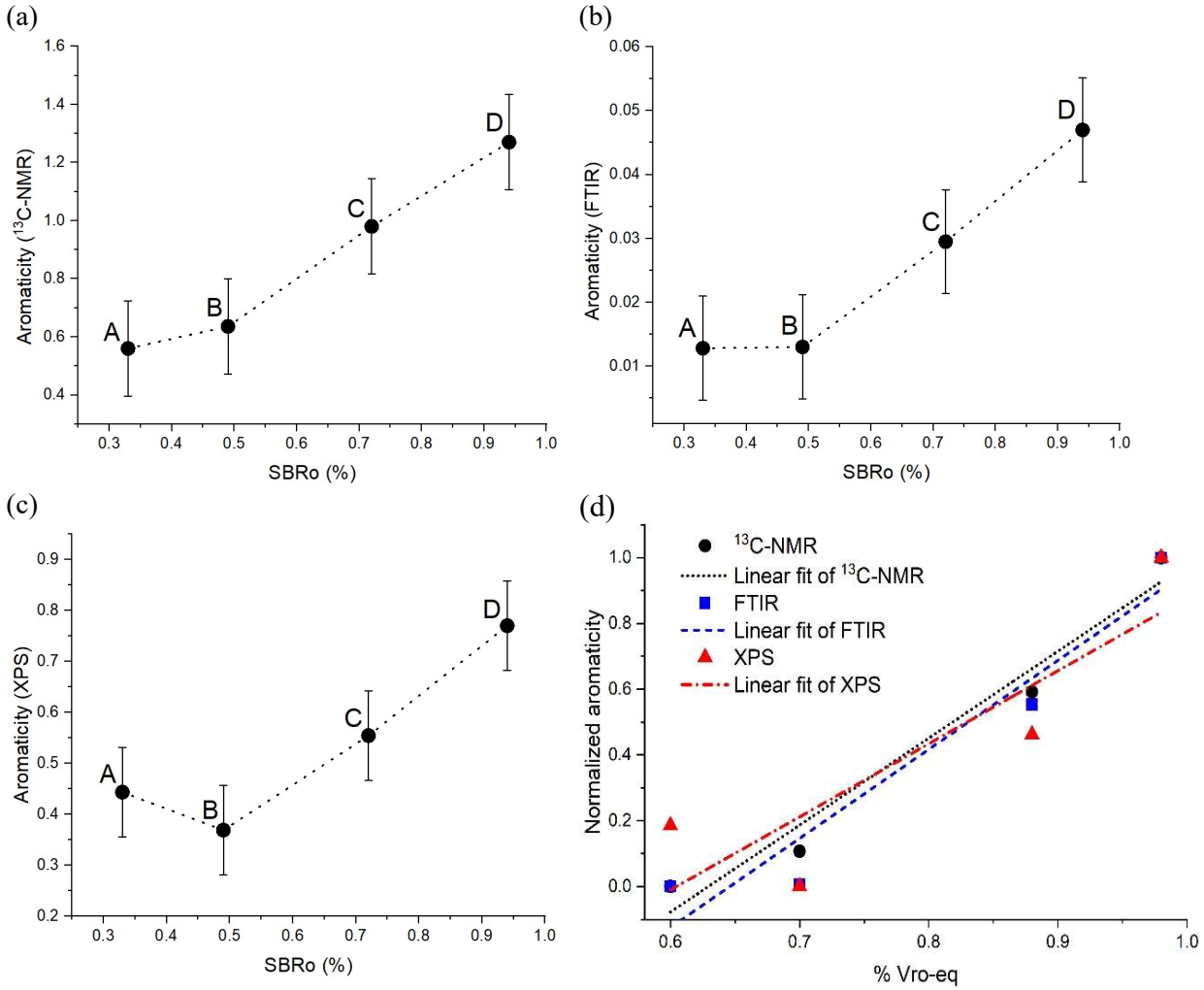

Figure 5. The aromatic carbon structural changes by thermal maturity. The aromaticity (aromatic carbon/aliphatic carbon) was calculated from (a) ^{13}C−NMR [$f_{ar}^{H} + f_{ar}^{B} + f_{ar}^{S} + f_{ar}^{P}$], (b) FTIR [$I_{(3130-3070)}/(I_{(2970-2950)}+I_{(2935-2915)})$], and (c) XPS. (d) Comparison of aromaticity slop trends (linearly fitted). Error bars represent standard errors.

Figure 5 depicts the aromatic carbon as investigated by three different analytical methods, ^{13}C−NMR, FTIR, and XPS. Figures 5a−c verifies our finding that higher maturity kerogen overall tends to have more amount of aromatic carbon. This is also compatible with the ^{1}H−NMR result, which infers to the ratio of aliphatic protons to the aromatic ring compared to the rest of protons. With an increase of maturity (sample A to D), the spectrum becomes sharper and has diminished intensity in the range of the aliphatic protons between 0.5 to 4.3 ppm, which represents the abundance of aromatic structure. This observation is collectively acceptable excluding sample B with the amount of aromatic carbon of XPS being comparatively 13% lower than the one of ^{13}C−NMR.

FTIR results also proposes that the aromaticity value of sample B is similar to sample A, which is different than the overall observed trend. This latest outcome can support lower A-factor values for Sample B compared to Sample A, as seen in Figure 4d. In addition, the degree of aromaticity (Figure 5d) estimated from three techniques (^{13}C−NMR, FTIR, and XPS) strongly confirms that the aromaticity is increasing. Notably, we found that that based on the aromaticity results there is relatively a considerable rift between pre−oil and oil window stage samples. Following to the oil window stage, the amount of aromatic carbon fairly increases, as well as the rate of change in aromaticity as seen by the slope of the curve which is found higher through advancing thermal maturity in the oil generation window.

Based on the results, the structural changes of the Bakken kerogen, coupled with hydrocarbon generation, is affected by the C−C BDE during the thermal maturation process. Due to the weaker BDE between α−β carbons than α−aromatic carbons, breaking the aliphatic chain bond leads to both the hydrocarbon generation and the aromatic abundant structure in kerogen backbone. In other words, during the thermal maturation, the comparatively light hydrocarbon was detached, and the remaining kerogen backbone became relatively solid−state organic compound having abundant aromatic structure and well organized rings.

3.5. Heteroatoms

The loss of oxygen functional groups drives early structural changes. Because the oxygen−related carbon bonds have relatively weak BDE, the carboxyl and carbonyl groups can be easily defunctionalized [21,34]. In our study, the results revealed that kerogen maturation involves

relatively bulky oxygen−related carbon reduction at the early stage of maturation (pre−oil window) then it increases in oil window stage, which is verified by ^{13}C−NMR and XPS in Tables 2 and 3.

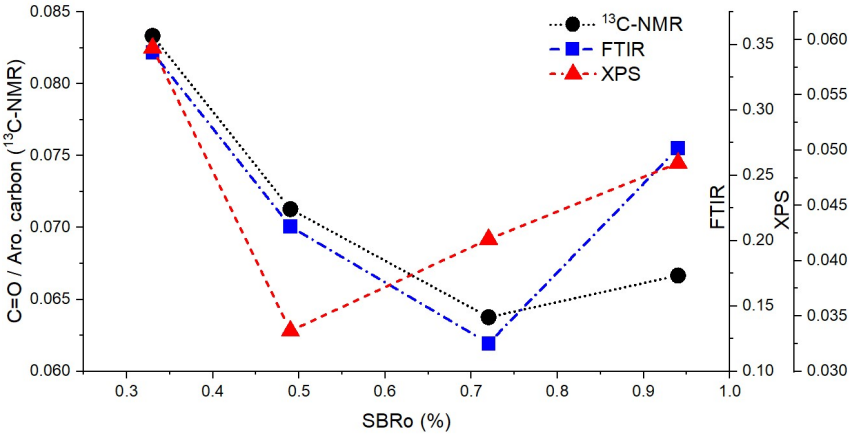

Figure 6. The ratios of C=O/aromatic carbon were estimated from ^{13}C−NMR, FTIR, and XPS results, which were calculated by $f_a^C/(f_{ar}^H+f_{ar}^B+f_{ar}^S+f_{ar}^P)$, C−factor $[I_{(1650-1750)}/(I_{(1650-1750)}+I_{(1615-1580)})]$, and [(total oxygen) x (C=O and C−O=O mole fraction)/(aromatic carbon)], respectively.

The changes in the ratios of C=O/aromatic carbon were investigated by three methods (^{13}C−NMR, FTIR, and XPS) depicted in Figure 6. Because it is difficult to analyze the organic oxygen group from ^{13}C−NMR [29], the comparison of three methods is presented in a same graph to help us better understand and verify the results. As thermal maturity increases, first the ratio of C=O/aromatic carbon decreases regardless of the method, along with the ratio of carbonyl/carboxyl functional groups to aromatic carbon which also was found to reduce at the early stages of maturation. Then, in the oil−window stage (sample C−D), the ratio of C=O/aromatic carbon starts to rise showing that the amount of oxygen estimated in sample D to become higher than sample C. Although most oxygen−containing functional groups will be expelled from the organic matter during the initial stages of thermal maturation, the results exhibit an unexpected increase in the oxygen content of the functional groups in the higher maturity ranges of kerogen. This can be explained by the enrichment of oxygen through addition of oxygen from inorganic mineral or water (interstitial water) impurities as thermal maturity increases which is also observed in other studies [8,22,34]. It's also expected that the formation of insoluble

pyro−bitumen, which is highly oxidized as thermal maturity advances, may lead to an unexpected increase of C=O/aromatic carbon ratio in higher thermal maturations.

Organic sulfur in kerogen from XPS studies clearly shows that the amount of sulfur decreases from the early stage of the maturation process. Sample A contains the largest number of sulfur (2.8 sulfur per 100 carbon), whereas sample B−D measured with lower quantities of sulfur (1.4, 1.1, and 0.7 per 100 carbons, respectively). This observed phenomenon is due to fact that the maturation process entails the depolymerization of kerogen structure by breaking the weak bonds (C−O and C−S) generating heavy soluble bitumen compounds [37]. Organic sulfur in aliphatic and aromatic compounds, sulfoxide, and SO_x (sulfate/sulfite/sulfone) in addition to inorganic sulfur and pyrite appear in all spectra as shown in Table 3. Organic nitrogen as detected by XPS revealed that it mainly contains pyrrolic, pyridinic, quaternary, and amino, is detected at different peaks based on their energy positions [5,29]; the nitrogen data for each kerogen samples is listed in Table 3. Based on the XPS results from the Bakken kerogen samples, we deduced that a variety of nitrogen associated compounds can exist in the samples regardless of the thermal maturation stage. This means, we were not able to establish a meaningful change in nitrogen quantity in our samples and further study is required to investigate the role of organic nitrogen during depolymerization of kerogen structure.

Generally speaking, based on the results, the weak bonds in the complex structure of kerogen start to detach containing bonds between C−O, and C−S at the early stages of maturation. These bond−breaking reactions would lead to the generation of H_2S gas, NSO compounds, and heavy soluble compound (bitumen). It needs to reiterate that the structural and chemical evolution of the Bakken kerogen involves defunctionalization of heteroatom functional groups, coupled with an increase in cross−linked carbon in the residual higher maturity kerogen.

5. Conclusions

This study shows how hydrocarbon generation can impose changes in the source rock organic compound structure during the maturation process. The analysis of extracted kerogen through spectroscopic techniques (^{1}H & ^{13}C−NMR, XPS, and FTIR) was used to determine chemical contents and molecular structures as maturation advances. This study will enable us to better model

separation and capture processes in shale plays via theoretical methods. Based on the results the following conclusions can be made:

- The structural changes of kerogen pertaining to the abundance of the aromatic and aliphatic chain length correlates well with the maturity of kerogen. Based on the aliphatic carbon chain that is detected in kerogen structure by ^{1}H & $^{13}C-NMR$ and FTIR, the ratio of CH_3/CH_2 increases when the maturity increases accompanied with the shorter aliphatic chain length.
- In contrast to aliphatic carbon, the aromatic carbon structure becomes more abundant in higher maturity and oil window stage. All three techniques ($^{13}C-NMR$, XPS, and FTIR) confirms an increasing trend similar to aromaticity with the same rate of changes. Also, a considerable discrepancy between pre−oil window and oil window stage regarding aromaticity was observed.
- Kerogen maturation causes the relatively bulky oxygen compounds reduction at the early stage of maturation (pre−oil window) with an increase in the oil window stage, based on $^{13}C-NMR$ and XPS results. In addition, the ratio of carbonyl/carboxyl functional groups to aromatic carbon shows an increase in the oil window stage (mature kerogen). This may be driven by contamination from inorganic oxygen in mineral or interstitial water impurities. Besides, the formation of insoluble oxygen−rich pyro−bitumen can lead to enrichment of the C=O/aromatic carbon ratio.
- The reduction of sulfur in kerogen was observed, as the level of maturity increases, mostly in SO_x forms. Finally, the XPS results exhibited that the diverse form of nitrogen could exist regardless of the thermal maturation stage however, further investigations of heteroatoms is necessary for better understanding of changes in NSO content as a function of thermal maturity.

Reference

(1) Durand, B. Sedimentary Organic Matter and Kerogen. Definition and Quantitative Importance of Kerogen. Kerogen, Insoluble Organic Matter from Sedimentary Rock, Editions technips 1980, 13–34.
(2) Rullkötter, J., & Michaelis, W. The Structure of Kerogen and Related Materials. A Review of Recent Progress and Future Trends. Org. Geochem 1990, 16(4–6), 829–852.

(3) Lee, H.; Shakib, F. A.; Shokouhimehr M.; Bubach, B.; Kong, L.; Ostadhassan, M. Optimal separation of CO2/CH4/Brine with amorphous Kerogen: A thermodynamics and kinetics study. J. Phys. Chem. C 2019, 123, 34, 20877–20883.
(4) Vandenbroucke, M.; Largeau, C. Kerogen Origin, Evolution and Structure. Org. Geochem 2007, 38, 719–833.
(5) Tong, J.; Han, X.; Wang, S.; Jiang, X. Evaluation of Structural Characteristics of Huadian Oil Shale Kerogen Using Direct Techniques (Solid–State 13C NMR, XPS, FT–IR, and XRD). Energy Fuels 2011, 25, 4006–4013.
(6) Tong, L.; Jiang, X.; Han, X.; Wang. Evaluation of the macromolecular structure of Huadian oil shale kerogen using molecular modeling. Fuel 2016, 181, 330–339.
(7) Clough, A.; Sigle, J. L.; Jacobi, D.; Sheremata, J.; White, J. L. Characterization of Kerogen and Source Rock Maturation Using Solid–State NMR Spectroscopy. Energy Fuels 2015, 29, 6370–6382.
(8) Lis, G.P.; Mastalerz, M.; Schimmelmann, A; Lewan, M.D.; Stankiewicz B.A. FTIR absorption indices for thermal maturity in comparison with vitrinite reflectance R0 in type–II kerogens from Devonian black shales. Org. Geochem. 2005, 36, 1533–1552.
(9) Khatibi, S.; Ostadhassan, M.; Tuschel, D.; Gentzis, T.; Bubach, B.; Carvajal–Ortiz, H. Raman spectroscopy to study thermal maturity and elastic modulus of kerogen. Int. J. Coal Geol. 2018, 185, 103–118.
(10) Wei, Z.; Gao, Z.; Zhang, D.; Da, J. Assessment of Thermal Evolution of Kerogen Geopolymers with Their Structural Parameters Measured by Solid–State 13C NMR Spectroscopy. Energy Fuels 2005, 19, 240–250.
(11) Lee, H.; Ostadhassan, M.; liu, K.; Bubach, B. Developing an Amorphous Kerogen Molecular Model Based on Gas Adsorption Isotherms, 2019. [Online early access]. DOI:10.26434/chemrxiv.7965152. Published Online: April 09, 2019. https://chemrxiv.org/s/dbfe102258d971e948f6
(12) Khatibi, S.; Ostadhassan, M.; Aghajanpour, A. Raman spectroscopy: an analytical tool for evaluating organic matter. J Oil Gas Petrochem Sci. 2018, 1, 28–33.
(13) Renault, M.; Cukkemane, A.; Baldus, M. Solid-State NMR Spectroscopy on Complex Biomolecules. Angew. Chem. Int. Ed.2010, 49, 8346 – 8357.
(14) Minor, E. C.; Swenson, M. M.; Mattson, B. M.; Oyler, A. R. Structural characterization of dissolved organic matter: a review of current techniques for isolation and analysis. Environ. Sci.: Processes Impacts 2014, 16, 2064-2079.
(15) VanderHart, D. L.; Retcofsky, H. L. Estimation of Coal Aromaticities by Proton–Decoupled Carbon–13 Magnetic Resonance Spectra of Whole Coals. Fuel 1976, 55, 202–204.
(16) Hatcher, P.G.;Wilson, M.A.; Vassallo, A.M.; Lerch, H.E. Studies of Angiospermous Wood in Australian Brown Coal by Nuclear Magnetic Resonance and Analytical Pyrolysis: New Insights into the Early Coalification Process. Int. J. Coal Geol. 1989, 13, 99–126.
(17) Wang, S.; Tang, Y.; Schobert, H. H.; Guo, Y.; Su, Y. FTIR and 13C NMR Investigation of Coal Component of Late Permian Coals from Southern China. Energy Fuels 2011, 25, 5672–5677.

(18) Kelemen S. R., Afeworki, M., Gorbaty, M. L. Characterization of Organically Bound Oxygen Forms in Lignites, Peats, and Pyrolyzed Peats by X–ray Photoelectron Spectroscopy (XPS) and Solid–State 13C NMR Methods. Energy Fuels 2002, 16, 1450–1462.
(19) Wang, Q.; Hou, T.; Wu, W.; Yu, Z.; Ren, S.; Liu, Q.; Liu, Z. A Study on the Structure of Yilan Oil Shale Kerogen based on Its Alkali–Oxygen Oxidation Yields of Benzene Carboxylic Acids, 13C NMR and XPS. Fuel Process. Technol. 2017, 166, 30–40.
(20) Lin, R.; Ritz, G. P. Studying Individual Macerals using i.r. Microspectroscopy, and Implications on Oil versus Gas/Condensate Proneness and "low–rank" Generation. Org. Geochem. 1993, 20, 695–706.
(21) Salmon E.; Behar F.; Lorant F.; Hatcher P.G.; Marquaire P.M. Early Maturation Processes in Coal. Part 1: Pyrolysis Mass Balance and Structural Evolution of Coalified Wood from the Morwell Brown Coal Seam. Org. Geochem. 2009, 40, 500−509.
(22) Michels, R.; Langlois, E.; Ruau, O.; Mansuy, L.; Elie, M.; Landais P. Evolution of Asphaltenes during Artificial Maturation: A Record of the Chemical Processes. Energy Fuels 1996, 10, 39–48.
(23) Abarghani, A.; Ostadhassan, M.; Gentzis, T.; Carvajal–Ortiz, H.; Bubach, B. Organofacies study of the Bakken source rock in North Dakota, USA, based on organic petrology and geochemistry. Int. J. Coal Geol. 2018, 188, 79–93.
(24) Khatibi, S.; Ostadhassan, M.; Tuschel, D.; Gentzis, T.; Carvajai–Ortiz, H. Evaluating Molecular Evolution of Kerogen by Raman Spectroscopy: Correlation with Optical Microscopy and Rock–Eval Pyrolysis. Energies 2018, 11, 1406.
(25) Wei, Q.; Tang, T. 13C–NMR Study on Structure Evolution Characteristics of High–Organic–Sulfur Coals from Typical Chinese Areas. Minerals 2018, 8, 49.
(26) Wang, Q.; Cui, D.; Wang, P.; Bai, J.; Wang, Z.; Liu, B. A Comparison of the Structures of > 300 °C Fractions in Six Chinese Shale Oils Obtained from Different Locations using 1H NMR, 13C NMR and FT–IR. Fuel 2018, 211, 341–352.
(27) Heide, P.V.D. X–ray photoelectron spectroscopy–An introduction to principles and practices. Wiley, 2012.
(28) Coates, John Interpretation of Infrared Spectra, A Practical Approach. Encyclopedia of Analytical Chemistry 2006, doi.org/10.1002/9780470027318.a5606
(29) Kelemen S. R., Afeworki, M., Gorbaty, M. L., Sansone, M., Kwiatek, P. J., Walters, C. C., Freund, H., Siskin, M.: Direct Characterization of Kerogen by X–ray and Solid–State 13C Nuclear Magnetic Resonance Methods. Energy Fuels 2007, 21, 1548–1561.
(30) Borrego, A. G.; Blanco, C. G.; Prado, J. G.; Diaz, C.; Guillen, M. D. 1H NMR and FTIR Spectroscopic Studies od Bitumen and Shale Oil from Selected Spanish Oil Shales. Energy Fuels 1996, 10, 77–84.
(31) Premovic, P. I.; Jovanovic, Lj. S.; Michel, D. Solid–State 13C and 1H NMR in Kerogen Research: Uncertainty of Aromaticity Estimation. Appl. Spectrosc. 1992, 46, 1750–1752.
(32) Kelemen, S.R.; Rose, K.D.; Kwiatek, P.J. Carbon aromaticity based on XPS $\prod$ to $\prod^*$ signal intensity. Appl. Surf. Sci. 1993, 64, 167–173.

(33) Yao, X.; Hou, X.; Wu, G.; Xu, Y.; Xiang, H.; Jiao, H.; Li, Y. Estimation of C–C Bond Dissociation Enthalpies of Large Aromatic Hydrocarbon Compounds Using DFT Methods. J. Phys. Chem. A 2002, 106, 7184–7189.
(34) Craddock, P. R.; Bake, K D.; Pomerantz, A. E. Chemical, Molecular, and Microstructural Evolution of Kerogen during Thermal Maturation: Case Study from the Woodford Shale of Oklahoma. Energy Fuels 2018, 32, 4859–4872.
(35) Takeda, N.; Asakawa, T. Study of petroleum generation by pyrolysis—I. Pyrolysis experiments by Rock–Eval and assumption of molecular structural change of kerogen using 13C–NMR. Appl. Geochem. 1988, 3, 441–453.
(36) Manka, M. J.; Brown, R. L.; Stein, S. E. Flow ESR and Static Studies of the Decomposition of Phenyl–Substituted Ethanes. J. Phys. Chem. 1985, 89, 5421–5427.
(37) Behar, F.; Lorant, F.; Lewan, M. Role of NSO Compound during Primary Cracking of a Type II Kerogen and a Type III Lignite. Org. Geochem. 2008, 39, 1–22.